Nigerian Research Journal of Engineering and Environmental Sciences 3(1) 2018 pp. 75-86

Nigerian Research Journal of Engineering and Environmental Sciences
Journal homepage: www.rjees.com

Original Research Article

THERMOGRAVIMETRIC AND SPECTROSCOPIC STUDIES OF CARBON DEPOSITED ON SBA-15 SUPPORTED NICKEL (Ni) CATALYST DURING CARBON DIOXIDE (CO_2) REFORMING OF METHANE

***[1,2]Omoregbe, O., [1]Ihoeghian, N.A., [1]Edokpayi, O., [1]Ossai, J.E. and [1,3]Awelenje, Q.A.**

[1]Department of Chemical Engineering, University of Benin, PMB 1154, Benin City, Edo State, Nigeria.
[2]Faculty of Chemical & Natural Resources Engineering, Universiti Malaysia Pahang, Lebuhraya Tun Razak, 26300 Gambang, Kuantan, Pahang, Malaysia.
[3]Tosett Agro Industries Limited, 112 Funsho Willam Avenue, Surulere Agege, Lagos, Nigeria.
*osaze.omoregbe@uniben.edu

ARTICLE INFORMATION

Article history:
Received 14 May, 2018
Revised 18 May, 2018
Accepted 20 May, 2018
Available online 30 June, 2018

Keywords:
Boudouard reaction
Ni/SBA-15
Gasification
Catalyst decay
Silanol group

ABSTRACT

The heterogeneity and amount of carbon deposited on Santa Barbara Amorphous-15 (SBA-15) supported Nickel (Ni) catalyst synthesised by incipient wetness impregnation method during carbon dioxide (CO_2) reforming of methane (CH_4) have been studied. The reforming process was performed in a fixed-bed tubular quartz reactor at 1023 K for up to 240 min under atmospheric pressure, and with varying CO_2/CH_4 feed ratios of 1:1–3:1 and 1:1–1:3, respectively. The activity of Ni catalyst was found to be influenced by the reactant's feed ratios. An increase in CO_2/CH_4 feed ratio positively affected CH_4 conversion whilst a steady drop in CO_2 conversion was observed. On the other hand, H_2 yield declined with increase in CO_2/CH_4 feed ratio, and CO yield increased, indicating the occurrence of side reactions such as reverse water-gas shift, and carbon gasification reactions. When the amount of CH_4 in the feed was raised above the stoichiometric value, a rapid deactivation of the catalyst was observed. Post-characterization analysis of the spent catalysts revealed that carbon deposition was directly proportional to reactant's feed ratio. Evidently, the least amount of carbon was observed at CO_2/CH_4 ratio of 2.5:1 while coke formation was greatly favoured at higher CH_4 composition in the feed.

1. INTRODUCTION

The deactivation of catalysts in various chemical reactions, which is the loss of catalytic performance over time, has been a serious predicament in catalysts utilisation for industrial-scale processes (Argyle and Bartholomew, 2015). Catalyst decay normally leads to process shutdown and a regular replacement of the used catalysts by fresh ones, a practice that costs industries to the tune of billions of dollars per annum (Argyle and Bartholomew, 2015). Catalysts stability differ appreciably; for instance, catalysts could

deteriorate in the order of seconds in the case of cracking catalysts, while iron catalyst may be active for about 5–10 years in ammonia synthesis (Bartholomew, 2001). However, the degradation of all catalysts is unavoidable. Catalyst mortality mainly occurs via the sintering of active metal and carbon formation over the surface (Estephane et al., 2015). Carbon may be formed on the catalyst surface in different forms, with each possessing special characteristics. Under conditions of CO_2 reforming of methane (CRM) (Equation (1)), carbon deposition over catalyst results mainly from the Boudouard reaction (Equation (2)), and CH_4 cracking (Equation (3)), with each reaction developing different kinds of carbon (Al-Fatesh and Fakeeha, 2012; Budiman et al., 2012; Pakhare and Spivey, 2014; Usman et al., 2015). Other side reactions favouring carbon formation are CO_2 and CO reduction (Equations (4) and (5), respectively) (Zhang et al., 2008; Ayodele et al., 2015). Whereas Boudouard reaction is thermodynamically favoured at lower temperatures below 973 K, CH_4 decomposition is favoured at temperatures above 826 K (Therdthianwong et al., 2008; Al-Fatesh and Fakeeha, 2012; Budiman et al., 2012; Bredesen et al., 2015).

$$CH_4 + CO_2 \rightarrow 2CO + 2H_2 \qquad (\Delta H^0_{298K} = 247.3\,\text{kJ mol}^{-1}) \tag{1}$$

$$2CO \leftrightarrow C + CO_2 \qquad (\Delta H^0_{298K} = -172.4\ \text{kJ mol}^{-1}) \tag{2}$$

$$CH_4 \rightarrow C + 2H_2 \qquad (\Delta H^0_{298K} = 75.0\,\text{kJ mol}^{-1}) \tag{3}$$

$$2CO_2 + 2H_2 \leftrightarrow C + 2H_2O \qquad (\Delta H^0_{298K} = -90.0\ \text{kJ mol}^{-1}) \tag{4}$$

$$CO + H_2 \leftrightarrow C + H_2O \qquad (\Delta H^0_{298K} = -131.3\ \text{kJ mol}^{-1}) \tag{5}$$

Carbon formed during reforming processes may be physically adsorbed in multilayers or be chemically adsorbed firmly as a monolayer, and in either case can obstruct reactants from the metal surface sites. It can also completely engulf a metal particle and thus totally deactivate that particle, and could possibly occlude micro- and mesopores, thereby preventing reactants from reaching the active metal crystallites inside these pores (Rostrup-Nielsen, 1997). The forms of carbon deposited during reforming conditions are greatly dependent on the operating temperatures. Cα is formed from CO segregation or hydrocarbon cracking and can be converted to another reactive form that is polymeric (C_β). Both Cα and C_β are reactive and amorphous carbons formed at low temperatures and when subjected to high temperatures (>773 K) for a long duration, are converted to less reactive graphitic (C_C) (Bartholomew, 1982). The carbides, (Cγ), or the whisker-like or vermicular carbon (Cv) forms of carbon are produced from the dissolution of carbon into the greater part of the metal. For reforming reactions carried out at temperatures above 973 K, the type of carbon formed on the catalyst surface may be (C_v) or (C_c) (Pechimuthu et al., 2007). The C_v whisker carbons are graphitic and are considered to possess equivalent diameter as the metal crystal (Ginsburg et al., 2005). Whiskers which are cylindrical in shape are generated owing to the presence of a diffused carbon concentration gradient in the metal crystal (Ginsburg et al., 2005). The C_c graphitic films are dispersed through the Ni particle surface, developing ordered graphite layers parallel to the metal-carbon interface. Indeed, detailed mechanisms of coking and carbon deposition on metal catalysts from CO and hydrocarbons can be found elsewhere (Bartholomew, 2001).

Since reactive carbons can be oxidized by the availability of oxygen in the catalyst framework, the net carbon deposits on metals during reactions such as methanation, steam-reforming, catalytic reforming, Fischer–Tropsch synthesis, and methanol synthesis are dependent on the difference in the rates of formation (r_f) and gasification (r_g) of carbon. Generally, rate of deactivation is the difference between the rates of formation and rate of gasification. No carbon will be deposited when formation rate is less than or equal to the gasification rate, and vice versa. Both rates of carbon formation and gasification grow exponentially with temperature while the difference between them fluctuates significantly with temperature owing to the variations in pre-exponential factors and activation energies (Bartholomew, 2001).

Nevertheless, the amount of coking during dry reforming processes can be controlled by adjusting the conditions under which the reaction is carried out. Indeed, few studies have reported the influence of operating parameters on coking and catalyst deactivation (Al-Fatesh and Fakeeha, 2012; Gaur et al., 2012; Serrano-Lotina and Daza, 2014; Ayodele et al., 2015; Khajenoori et al., 2015). This study evaluated the influence of reactants feed ratio on coke formation over 10%Ni/SBA-15 catalyst under dry reforming conditions. Subsequently, the heterogeneity and quantity of carbon deposited on the used catalyst after CRM were evaluated by temperature-programmed oxidation technique and Fourier transform infrared (FTIR) spectroscopy, respectively.

2. MATERIALS AND METHODS

2.1. Catalyst Preparation

SBA-15 support was synthesised according to the method reported in our previous work (Omoregbe et al., 2016). In a typical synthesis, 10.0 g of a nonionic triblock copolymer (Pluronic P-123) was dissolved in 260 mL of HCl solution with regulated pH of approximately 1 and stirred at 303 K. Afterwards, 20 g of tetraethyl orthosilicate (TEOS) was added dropwise into the P-123 solution with stirring at 310 K for 24 h. The solid product was recovered, washed with deionized water, and dried overnight at 373 K. Finally, the sample was calcined in air by gradually increasing the temperature from room temperature to 823 K at a rate of 2 K min^{-1} for 6 h. 10%Ni/SBA-15 catalyst was prepared via the incipient wetness impregnation method. This preparation technique involved the preliminary dissolution of nickel nitrate hexahydrate $Ni(NO_3)_2.6H_2O$; Sigma-Aldrich), which is a precursor for Ni, in deionized water to form a salt solution. Subsequently, SBA-15 was introduced into the above solution in a rotary evaporator (BÜCHI Rotavapor R-200) where the mixture was stirred at 338 K for 2 h under vacuum until the metal precursor was appreciably incorporated into the support. The catalyst was dried in an oven at 373 K overnight and subjected to calcination in air at 973 K for 5 h with a heating rate of 2 K min^{-1}.

2.2. Catalyst Characterization

Surface areas and pore structures of both support and catalyst were determined by a Micromeritics ASAP-2010 analyser using N_2 adsorption- desorption isotherms data obtained at 77 K. Prior to the tests, both the support and catalyst were degassed at 573 K for 1 h in order to remove moisture contents. The specific surface areas were estimated from the isotherms employing the Brunauer–Emmett–Teller (BET) method, and the pore distribution and the pores cumulative volumes were determined using the Barret–Joyner–Halenda (BJH) technique from the desorption curves of the N_2 isotherms. XRD patterns were conducted with 2θ ranging from 3° to 85° by a Rigaku Miniflex II system using Cu Monochromatic X-ray radiation (with wavelength, λ = 1.5418 Å) at 30 kV and 15 mA. The imaging of the samples was achieved by transmission electron microscope (TEM) with a JEOL-3010 electron microscope operating at 200 kV. In addition, Fourier transform infrared (FTIR) spectroscopic measurements were performed on a Fisher Scientific Nicolet iS5 Spectrometer fitted with an iD7 ATR component (Thermo Scientific) in order to investigate the surface chemistry of SBA-15 support, fresh, and spent Ni/SBA-15 catalysts. Post-reaction characterization analysis of the spent catalysts was carried out by temperature-programmed oxidation (TPO) measurements using TGA Q500 instrument and FTIR to measure the quantity of carbon formed over the catalyst surface.

2.3. Catalyst Testing

The catalytic performance of 10%Ni/SBA-15 catalyst was assessed in a fixed-bed continuous flow reactor made of quartz tube (I.D. = 7 mm, wall thickness = 1 mm) at 1023 K, and varying CO_2/CH_4 feed ratios of 1:1–3:1 and 1:1–1:3 under atmospheric pressure. Quartz wool was employed as the catalyst bed in the tubular reactor with about 0.15 g of catalyst mounted on the bed. Prior to the reforming reaction, the catalyst was

reduced in situ with a stream of H_2 (60 mL/min, 973 K) for 2 h. The flow rates of CH_4 and CO_2 reactants, which were mixed with N_2 inert gas before flowing to the inlet of the fixed-bed reactor, were accurately monitored using Alicat mass flow controllers. The total flow rate of gaseous feed stream ($CO_2/CH_4/N_2$) was set at 60 mL min^{-1} for all the reaction conditions. In order to ensure that the influence of mass and heat transport resistances is infinitesimal, catalyst with average particle size of 100-140 µm and gas hourly space velocity (GHSV) of 24 L g_{cat}^{-1} h^{-1} were employed. The effluent gas was analysed by GC-9860 gas chromatograph (Agilent 6890 Series GC system). The catalyst performance was determined in terms of CH_4 and CO_2 conversions, H_2 and CO yields, and H_2/CO ratio by applying the following equations:

$$X_i\ (\%) = \frac{F_i^{In} - F_i^{Out}}{F_i^{In}} \times 100\% \tag{6}$$

$$Y_{H_2}(\%) = \frac{F_{H_2}^{Out}}{2 \times F_{CH_4}^{In}} \times 100\% \tag{7}$$

$$Y_{CO}(\%) = \frac{F_{CO}^{Out}}{F_{CO_2}^{In} + F_{CH_4}^{In}} \times 100\% \tag{8}$$

$$\mathrm{H_2/CO\ ratio} = \frac{F_{H_2}^{Out}}{F_{CO}^{Out}} \times 100\% \tag{9}$$

Where X_i = Conversion of species i (%); F = Flow rate (mol s^{-1}); and Y_j = Yield of species j (%)

3. RESULTS AND DISCUSSION

3.1. Physicochemical Properties

The N_2 adsorption–desorption isotherms of SBA-15 support and 10%Ni/SBA-15 catalyst is depicted in Figure 1.

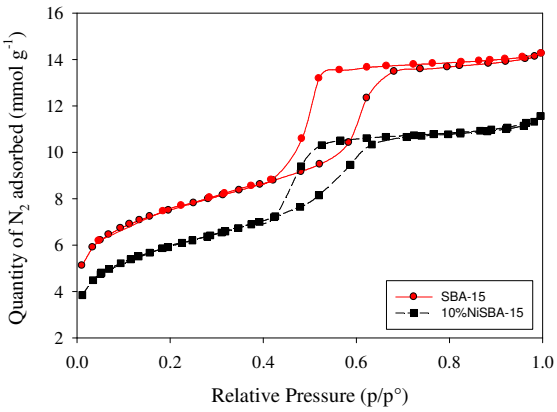

Figure 1: N_2 adsorption–desorption isotherms of freshly prepared SBA-15, and 10%Ni/SBA-15 catalyst

Notably, both samples displayed characteristic reversible-type IV isotherm, indicating that the mesoporous structures of the samples were preserved after the impregnation of nickel oxide into the SBA-15 support framework. These isotherms for SBA-15 and Ni catalyst are in agreement with other studies (Liu et al., 2008; Li et al., 2015). Additionally, the influence of incorporating nickel metal precursor into the support

was evident in the decrease from 550.05 to 444.96 m^2 g^{-1} surface area, and 0.49 to 0.40 cm^3 pore volume of the support. These results confirm the successful dispersion of NiO species into the pore system of SBA-15. However, the substantial shrinkage in the surface area and pore volume was noticed after the addition of Ni, which could be due to partial blockage of the pore entrances by NiO species (Naeem et al., 2014).

3.2. X-Ray Diffraction Analysis

The XRD patterns of SBA-15 support and 10% Ni/SBA-15 catalyst are shown in Figure 2. The obtained data were interpreted by the Joint Committee on Powder Diffraction Standards (JCPDS) database (JCPDS Powder Diffraction File, 2000). XRD patterns of both SBA-15 support and 10%Ni/SBA-15 catalyst revealed the existence of a silica phase of the SBA-15 support, which was somewhat noticeable in the 2θ region of 15–30° (JCPDS card No. 29-0085) (Liu et al., 2008; Li et al., 2015). This broad region (SiO_2 phase) found in both samples signifies that the pore configuration of the support was not destroyed during the impregnation of NiO into the framework of the SBA-15 support. In the case of the 10%Ni/SBA-15 catalyst, the characteristic peaks observed at 2θ = 37.3°, 43.3°, 63.0° and 75.5° may be attributed to the presence of crystalline NiO phase (JCPDS card No. 47-1049).

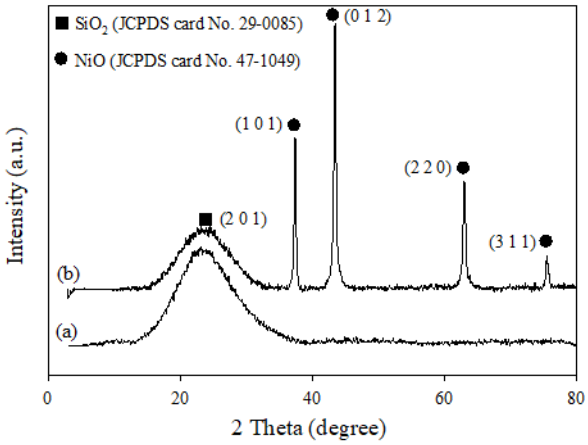

Figure 2: XRD patterns of calcined (a) SBA-15 support, and (b) 10%Ni/SBA-15 catalyst.

3.3. Fourier Transform Infrared Spectroscopic Measurements

Figure 3 describes the FTIR spectra of the SBA-15 support and 10% Ni/SBA-15 catalyst. Seven peaks were detected at 435.8, 568.5, 806.1, 952.7, 1076.1, 1658.5, and 3401.8 cm^{-1} for both samples. In Figure 3 (a), the absorption peaks at and below 1076.1 cm^{-1} are ascribed to the stretching and bending vibration of Si–O–Si bond (Li et al., 2014). Interestingly, there was a significant increase in the absorption peaks at absorption bands less than 1076.1 cm^{-1} after the impregnation of NiO (Figure 3 (b)). The increase in peak intensities at these bands (568.5, 806.1, 952.7 cm^{-1}) can be ascribed to the existence of inter-atomic vibrations among the NiO particles and silica groups (Saraswat and Pant, 2013; Rahemi et al., 2014). Absorption peaks at 1658.5 and 3401.8 cm^{-1} are assigned to the adsorbed water which interacts with silica species to form hydrogen bonded OH species and the stretching vibration of surface hydrogen-bonded Si–OH silanol group (Araújo et al., 2016). The similarities between the spectra lines of SBA-15 and 10% Ni/SBA-15 catalyst further verified that the mesoporous structure of the SBA-15 was not destroyed after the incorporation of NiO.

3.4. Transmission Electron Microscopic Measurements

Figure 4 shows the TEM results of the freshly prepared SBA-15 support and 10% Ni/SBA-15 catalyst. In Figure 4 (a), the TEM micrograph of SBA-15 shows the existence of wall channels, which are crucial for promoting metal dispersion. The active sites around the support boundaries enhance the reaction between the reactants and the active phase (Rahemi et al., 2014). Indeed, most of the NiO were well incorporated into the SBA-15 wall channels with few particles on the surface (Figure 4 (b)). These observations are in good agreement with the BET and XRD results.

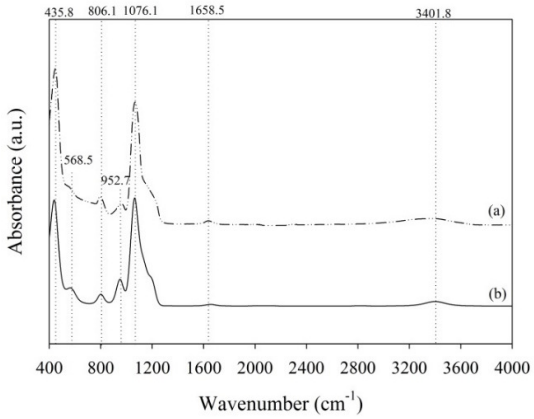

Figure 3: FTIR spectra of calcined (a) mesoporous SBA-15 support, and (b) 10%Ni/SBA-15 catalyst

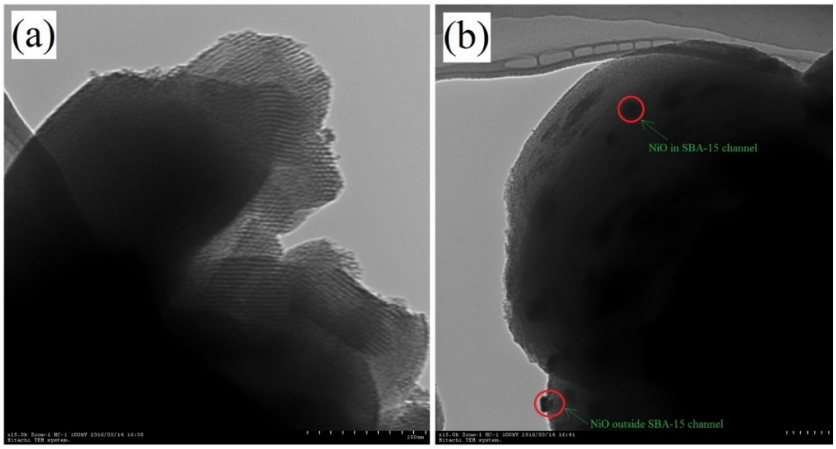

Figure 4: TEM images of freshly prepared (a) SBA-15 support, and (b) 10%Ni/SBA-15 catalyst.

3.5. Catalyst Activity Evaluation

Table 1 shows the activity tests results of the Ni/SBA-15 catalyst at varying CO_2/CH_4 feed ratios. As seen in Table 1, CO_2 conversion (X_{CO2}) was slightly higher than that of CH_4 conversion (X_{CH4}) at stoichiometric feed ratio. However, X_{CH4} increased with rising CO_2/CH_4 feed ratio until the optimum ratio of 2.5:1, whilst a steady drop in X_{CO2} was observed. The rise in X_{CH4} can be ascribed to CH_4 acting as a limiting reactant in the presence of higher CO_2 compositions. This condition possibly enhanced the activation of CH_4, which ordinarily has higher activation energy than CO_2 (Pakhare and Spivey, 2014).

Table 1: Influence of varying reactants compositions in feed on (a) CO_2 and CH_4 conversions, ratio of CH_4 reacted to H_2 yield, ratio of CO_2 reacted to CO yield and H_2/CO ratio at 1023 K.

CO_2/CH_4 feed ratio	X_{CH4}	X_{CO2}	X_{CH4}/Y_{H2} ratio	X_{CO2}/Y_{CO} ratio	H_2/CO ratio
Variation in CO_2 composition at constant CH_4					
1:1	91.1323	94.4252	1.0501	1.4457	0.9017
1.5:1	97.5964	79.7422	1.3212	1.1539	0.8146
2:1	98.3663	71.298	1.3785	1.0042	0.7202
2.5:1	98.841	61.1657	1.4064	0.7365	0.6389
3:1	98.1555	58.7193	1.4508	0.7007	0.5431
Variation in CH_4 composition at constant CO_2					
1:1	91.1323	94.4252	1.0211	1.4088	0.9017
01:1.5	71.3224	91.1351	1.0354	1.462	0.8634
1:2	48.9906	81.0897	1.7096	1.7729	0.8266
01:2.5	38.0601	77.4524	1.752	2.0124	0.8063
1:3	34.3892	76.4524	1.7942	2.2696	0.7929

Nikoo and Amin (2011) also reported similar observation during a study on thermodynamic analysis of CRM. The authors ascribed the decrease in CO_2 conversion at higher CO_2/CH_4 to the role of CH_4 as a limiting reactant that hindered the complete conversion of CO_2. Furthermore, H_2/CO ratio declined while the ratio of CH_4 consumed to H_2 yield increased at higher CO_2 in the feed. The decrease in H_2/CO ratio and the rise in the ratio of CH_4 conversion to H_2 yield were probably due to the occurrence of reverse water-gas shift (RWGS) reaction (Equation (10)), where the liberated H_2 from CH_4 decomposition is consumed. Additionally, the steam originating from RWGS reaction logically aided the gasification of carbon formed in CH_4 decomposition (Equation (11), thus increasing the amount of CO in the product stream. This occurrence can also explain the observed decrease in H_2/CO ratio at rising CO_2/CH_4 feed ratio. Thus, this study demonstrated that higher CO_2/CH_4 feed ratios favour RWGS reaction which will result in a decrease in H_2 yield and more carbon is gasified via steam from the RWGS.

$$CO_2 + H_2 \rightarrow CO + H_2O \quad \Delta H^0_{298K} = +41.0\, kJ\, mol^{-1} \tag{10}$$

$$C + H_2O \rightarrow CO + H_2 \quad \Delta H^0_{298K} = +131.3\, kJ\, mol^{-1} \tag{11}$$

However, when CH_4 composition in the feed was increased above CO_2 stoichiometric value, a rapid catalytic decay was observed. Usually, CO_2 can act as an oxidant (reverse of Eq. (2)) in which the carbon formed during the reforming reaction are oxidised into CO. However, at higher CH_4 compositions (lower CO_2/CH_4 ratios) the activation of CO_2 which is required for carbon oxidation would be low, and this will result in the formation of excess carbon (Pakhare & Spivey, 2014). Thus, the formation of excessive carbon either via CH_4 decomposition or Boudouard reaction at this condition is reasonably responsible for the rapid deactivation of the catalyst. Xu et al. (2010) also reported similar observation in their investigation over Ni-Co bimetallic catalyst. The study demonstrated that a growing amount of CH_4 in the reactants promoted the dissociation of CH_4 and carbon deposition, consequently, resulting in catalyst deactivation. Therefore, it can be urged that our results are in agreement with previous studies (Istadi & Amin, 2005; Serrano-Lotina & Daza, 2014; Khajenoori et al., 2015).

3.6. Carbon Study

3.6.1. TPO measurements

The heterogeneity and amount of carbon formed over the Ni catalyst during the dry reforming reaction were determined by the temperature-programmed oxidation technique (TPO). The required temperature for the complete oxidation of carbon is a function of the carbon bond strength to the catalyst's surface and this varies for different types of carbonaceous species (Castaño et al., 2012; Wolfbeisser et al., 2016). Generally, low oxidation temperatures are associated with the presence of amorphous carbon whilst elevated temperatures are associated with graphitic carbon owing to their higher bond strengths (Bartholomew, 2001; Selvarajah, Phuc, Abdullah, Alenazey, & Vo, 2016; Wolfbeisser et al., 2016). Figures 5 (a) and (b) represent the derivative weights and weight loss percent profiles, respectively, of the used catalysts after 240 min on-stream CRM at varying CO_2 feed ratio.

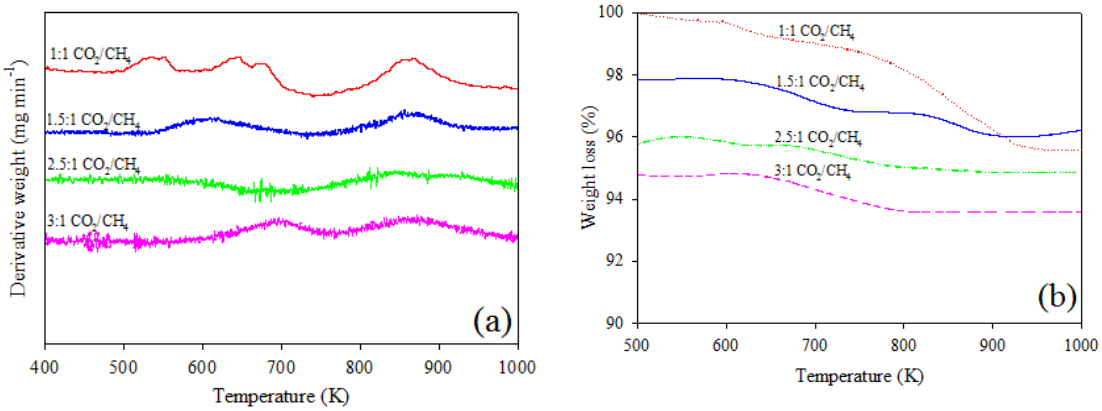

Figure 5: Derivative weight and percentage weight loss profiles for TPO results of spent 10%Ni/SBA-15 catalysts after 240 min on-stream CRM at temperature of 1023 K and varying CO_2 feed composition

As seen in Figure 5(a), the sample at CO_2/CH_4 feed ratio of 1:1 exhibited three oxidation peaks at 540 K, 650 K, and 856 K. The peaks at 540 K and 650 K can be ascribed to the oxidation of an amorphous carbonaceous species (Xu et al., 2009; Wu et al., 2014; Mehdi et al., 2017; Erdogan et al., 2018) while the peak at 856 K can be attributed to the oxidation of graphitic carbon (Bartholomew, 2001; Selvarajah et al., 2016; Wolfbeisser et al., 2016). Moreover, for samples with CO_2/CH_4 ratios of 1.5:1 and 2.5:1, two peaks were formed at 605 K and 856 K. The peak at 605 K can be credited to amorphous carbon while the peak at 856 K is ascribed to graphitic carbon (Xu et al, 2009; Wu et al., 2014; Mehdi et al., 2017; Erdogan et al., 2018). Lastly, the derivative profile of sample at a CO_2/CH_4 feed ratio of 3:1 showed two peaks at 694 K and 856 K that can be attributed to amorphous and graphitic carbons, respectively. The weight loss percent of the used catalysts at higher CO_2/CH_4 ratios (Table 2 and Figure 5 (b)) revealed that more carbon was deposited on the catalyst at a CO_2/CH_4 ratio of 1:1. However, the quantity of carbon deposited decreased with increasing CO_2 composition in feed until a ratio of 2.5:1, where the lowest amount of carbon was observed. These observations are in agreement with the activity test results as discussed earlier, corroborating the assertion that carbon gasification was favoured at higher CO_2/CH_4 ratios owing to enhanced RWGS reaction.

Table 2: Weight loss percent during TPO measurements of spent 10%Ni/SBA-15 catalysts after 240 min on-stream CRM at temperature of 1023 K at varying CO_2 and CH_4 feed compositions.

CO_2/CH_4 ratio	Weight loss (%)	CO_2/CH_4 ratio	Weight loss (%)
1:1	4.01	1:1	4.01
1.5:1	1.86	1:1.5	9.62
2.5:1	1.03	1:2.5	11.54
3:1	1.25	1:3	13.01

The derivative weights and weight loss percent profiles of the used catalysts at higher CH_4 compositions in the feed are shown in Figures 6 (a) and (b), respectively. Interestingly, intense peaks were observed for these samples at higher CH_4 compositions, proving the formation of a significant amount of carbon. The oxidation peak temperatures for these catalysts, which are around 856 K can be assigned to the oxidation of graphitic carbon (Bartholomew, 2001; Xu et al., 2009; Wu et al., 2014; Selvarajah et al., 2016; Wolfbeisser et al., 2016). The weight loss percent (Table 2 and Figure 6 (b)) showed that the amount of carbon deposited for the samples at higher CH_4 compositions (CO_2/CH_4 = 1:2.5 and 1:3) were greater than that of low CH_4 composition (CO_2/CH_4 = 1:1.5). These results show that the deactivation of the catalyst observed during the activity test was due to the formation of excess carbon which could not be gasified owing to deficient CO_2 in the CH_4-rich feed conditions.

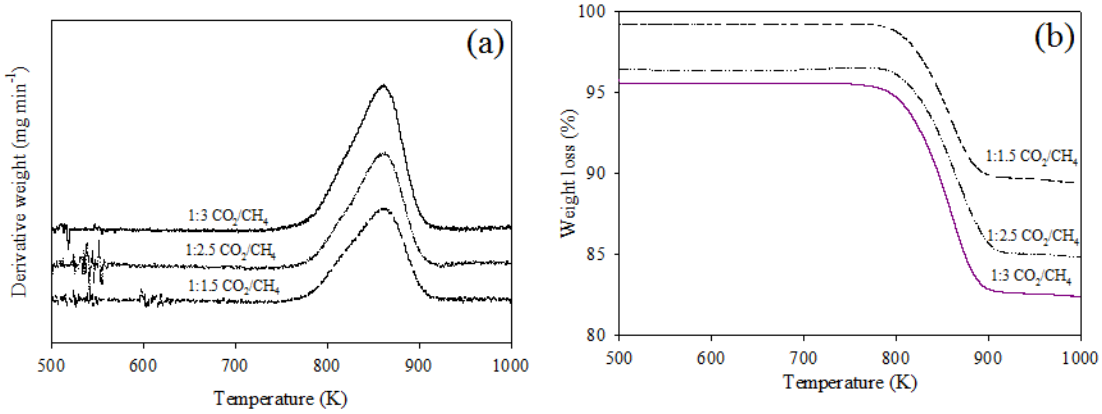

Figure 6: Derivative weight and percentage weight loss profiles for TPO results of spent 10%Ni/SBA-15 catalysts after 240 min on-stream CRM at temperature of 1023 K at varying CH_4 feed composition

3.6.2 FTIR measurements

Figures 7 (a) - (e) depict the FTIR results of spent catalysts after 240 min on-stream CRM at varying CH_4 compositions. As seen in the spectra of all the samples, the surface chemistry of the catalyst did not change significantly after the dry reforming reaction. Meanwhile, a new peak was detected in Figures 7 (b) and (c) at the absorption band of 2132.4 cm^{-1} that can be credited to C–H stretching mode of the hydrocarbon groups in the SBA-15 framework (Anandan & Rajendran, 2011; Majewski & Wood, 2014). An additional peak was observed in Figure 7 (b) at the absorption band of 2976.3 cm^{-1}, ascribable to the asymmetric stretching vibration of C–H bonds in methylene groups (CH_x) in the catalyst framework (Coates, 2000; Majewski & Wood, 2014). However, no new peaks were observed for Figures 7 (d) and (e), indicating there was enhanced gasification of carbon at higher CO_2 compositions (CO_2/CH_4 feed ratios of 2.5:1 and 3:1).

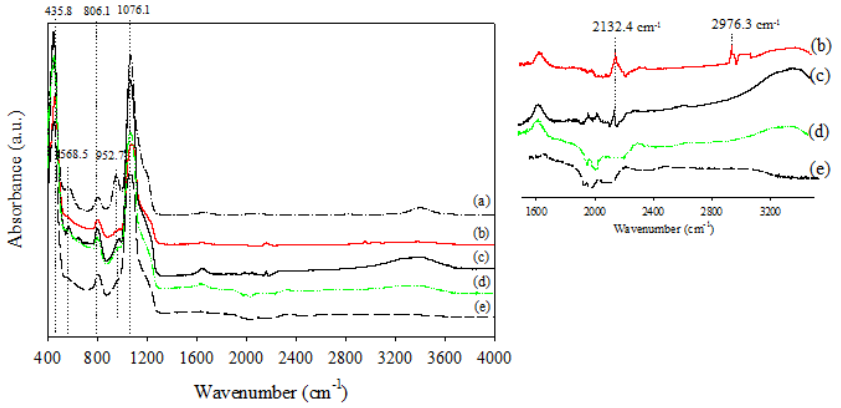

Figure 7: FTIR spectra of (a) fresh 10%Ni/SBA-15, and spent catalysts at CO_2/CH_4 feed ratio of (b) 1:1, (c) 1.5:1, (d) 2.5:1, and (e) 3:1 after 240 min on-stream CRM at 1023 K.

Interestingly, two characteristic bands at 2132.4 and 2976.3 cm^{-1} were detected for spent catalysts at higher CH_4 compositions (Figures 8 (c) – (e)). The peak at absorption band of 2132.4 cm^{-1} may be ascribed to the stretching mode of C–H bond in hydrocarbon groups bonded with the surface silica of SBA-15 while the peak at 2976.3 cm^{-1} may be attributed to the asymmetric stretching vibration of C–H bonds related to methylene groups (CH_x) which are connected to the aliphatic groups (Coates, 2000; Majewski & Wood, 2014). The observation of two new peaks confirms the presence of two different types of carbonaceous species, where the peak at lower absorption band (2132.4 cm^{-1}) is likely due to the presence of amorphous carbon and the peak at the higher band (2976.3 cm^{-1}) may be ascribed to the existence of graphite-like carbon groups.

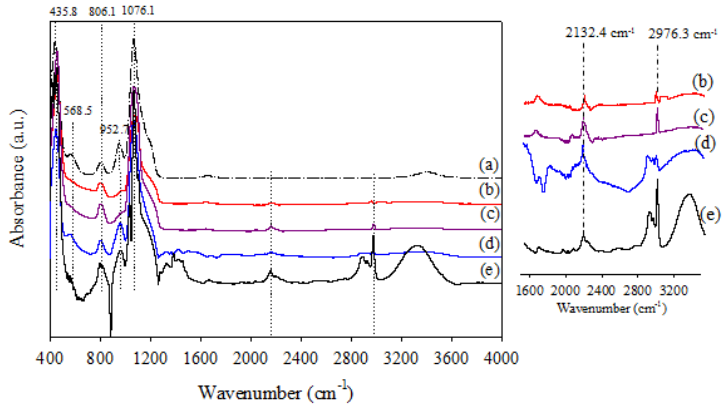

Figure 8: FT-IR spectra of (a) fresh 10%Ni/SBA-15, and spent catalysts at CO_2/CH_4 feed ratio of (b) 1:1, (c) 1:1.5, (d) 1:2.5, and (e) 1:3 after 240 min on-stream CRM at 1023 K.

4. CONCLUSION

10%Ni/SBA-15 catalyst was prepared by the incipient wetness impregnation method and characterised by BET, XRD, FTIR, and TEM techniques. The BET, XRD and TEM results revealed NiO was well dispersed in the SBA-15 support framework, while FTIR showed there was no significant alteration in the surface chemistry of the support after NiO impregnation. Catalyst activity tests results showed that 2.5:1 is the optimum CO_2/CH_4 feed ratio for maximum CH_4 conversion. An increase in CH_4 in the feed mixture at constant CO_2 greatly favoured carbon formation over the catalyst. The occurrence of coking during the CO_2

reforming reaction was further verified by TPO analysis and FTIR measurements. TPO results revealed that more carbonaceous materials were deposited at CH_4-rich feed conditions. Finally, the H_2/CO ratio was below unity for all conditions suggesting the occurrence of concomitant side reactions such as RWGS and carbon gasification reactions for H_2 consumption and CO formation, respectively.

5. ACKNOWLEDGEMENTS

The authors appreciate Universiti Malaysia Pahang for generously supporting this work through the Research Grant Scheme (Grant No: RDU160323). Osaze Omoregbe is also grateful to University of Benin for the study leave granted to him during the period of this research.

6. CONFLICT OF INTEREST

There is no conflict of interest associated with this work.

REFERENCES

Al-Fatesh, A. S. A., and Fakeeha, A. H. (2012). Effects of calcination and activation temperature on dry reforming catalysts. *Journal of Saudi Chemical Society, 16(1*), pp. 55–61.

Anandan, K. and Rajendran, V. (2011). Morphological and size effects of NiO nanoparticles via solvothermal process and their optical properties. *Materials Science in Semiconductor Processing, 14(1),* pp. 43–47.

Araújo, M. M., Silva, L. K. R., Sczancoski, J. C., Orlandi, M. O., Longo, E., Santos, A. G. D. and Cavalcante, L. S. (2016). Anatase TiO_2 nanocrystals anchored at inside of SBA-15 mesopores and their optical behavior. *Applied Surface Science, 389*, pp. 1137–1147.

Argyle, M. and Bartholomew, C. (2015). Heterogeneous Catalyst Deactivation and Regeneration: A Review. *Catalysts, 5(1),* pp. 145–269.

Ayodele, B. V, Khan, M. R. and Cheng, C. K. (2015). Syngas production from CO_2 reforming of methane over ceria supported cobalt catalyst: Effects of reactants partial pressure. *Journal of Natural Gas Science and Engineering, 27*, pp. 1016–1023.

Bartholomew, C. H. (1982). Carbon deposition in steam reforming and methanation. *Catalysis Reviews: Science and Engineering, 24(1*), pp. 67–112.

Bartholomew, C. H. (2001). Mechanisms of catalyst deactivation. *Applied Catalysis A: General, 212(1–2*), pp. 17–60.

Bredesen, R., Peters, T. A., Boeltken, T. and Dittmeyer, R. (2015). Pd-based membranes in hydrogen production for fuel cells. In F. G. and M. V. S. Annaland (Ed.), Process Intensification for Sustainable Conversion. Chichester, UK: John Wiley & Sons, Ltd.

Budiman, A. W., Song, S. H., Chang, T. S., Shin, C. H. and Choi, M. J. (2012). Dry Reforming of Methane Over Cobalt Catalysts: A Literature Review of Catalyst Development. *Catalysis Surveys from Asia, 16(4*), pp. 183–197.

Castaño, P., Gutiérrez, A., Hita, I., Arandes, J. M., Aguayo, A. T. and Bilbao, J. (2012). Deactivating species deposited on Pt-Pd catalysts in the hydrocracking of light-cycle oil. *Energy and Fuels, 26(3*), pp. 1509–1519.

Coates, J. (2000). Interpretation of Infrared Spectra, A Practical Approach. In *Encyclopedia of Analytical Chemistry* (pp. 10815–10837).

Erdogan, B., Arbag, H. and Yasyerli, N. (2018). SBA-15 supported mesoporous Ni and Co catalysts with high coke resistance for dry reforming of methane. *International Journal of Hydrogen Energy, 43(3*), pp. 1396–1405.

Estephane, J., Ayoub, M., Safieh, K., Kaydouh, M.-N., Casale, S. and Zakhem, H. E. (2015). CO_2 reforming of CH_4 over highly active and stable yRhNix/NaY catalysts. *Comptes Rendus Chimie, 18(3*), pp. 277–282.

Gaur, S., Pakhare, D., Wu, H., Haynes, D. J. and Spivey, J. J. (2012). CO_2 reforming of CH_4 over Ru-substituted pyrochlore catalysts: Effects of temperature and reactant feed ratio. *Energy and Fuels, 26(4*), pp. 1989–1998.

Ginsburg, J. M., Piña, J., El Solh, T. and De Lasa, H. I. (2005). Coke formation over a nickel catalyst under methane dry reforming conditions: Thermodynamic and kinetic models. *Industrial and Engineering Chemistry Research, 44(14*), pp. 4846–4854.

Istadi, & Amin, N. A. S. (2005). Co-Generation of C2 Hydrocarbons and Synthesis Gases from Methane and Carbon Dioxide: A Thermodynamic Analysis. *Journal of Natural Gas Chemistry, 14(3)*, pp. 140–150.

JCPDS Powder Diffraction File. (2000). International Centre for Diffraction Data. Swarthmore, PA.

Khajenoori, M., Rezaei, M. and Meshkani, F. (2015). Dry reforming over CeO_2-promoted Ni/MgO nano-catalyst: Effect of Ni loading and CH_4/CO_2 molar ratio. *Journal of Industrial and Engineering Chemistry, 21*, 717–722.

Li, D., Zeng, L., Li, X., Wang, X., Ma, H., Assabumrungrat, S. and Gong, J. (2015). Ceria-promoted Ni/SBA-15 catalysts for ethanol steam reforming with enhanced activity and resistance to deactivation. *Applied Catalysis B: Environmental, 176–177*, 532–541.

Li, J. F., Xia, C., Au, C. T. and Liu, B. S. (2014). Y_2O_3-promoted NiO/SBA-15 catalysts highly active for CO_2/CH_4 reforming. *International Journal of Hydrogen Energy, 39*, 10927–10940.

Liu, H., Wang, H., Shen, J., Sun, Y. and Liu, Z. (2008). Promotion effect of cerium and lanthanum oxides on Ni/SBA-15 catalyst for ammonia decomposition. *Catalysis Today, 131(1–4)*, pp. 444–449.

Majewski, A. J. and Wood, J. (2014). Tri-reforming of methane over Ni@SiO_2 catalyst. *International Journal of Hydrogen Energy, 39(24)*, pp. 12578–12585.

Mehdi, S., Meshkani, F. and Rezaei, M. (2017). Preparation of mesoporous nanocrystalline 10 % Ni/$Ce_{1-x}Mn_xO_2$ catalysts for dry reforming reaction. *International Journal of Hydrogen Energy,* 1–9.

Naeem, M. A., Al-Fatesh, A. S., Abasaeed, A. E. and Fakeeha, A. H. (2014). Activities of Ni-based nano catalysts for CO_2-CH_4 reforming prepared by polyol process. *Fuel Processing Technology, 122*, 141–152.

Omoregbe, O., Danh, H. T., Abidin, S. Z., Setiabudi, H. D., Abdullah, B., Vu, K. B. and Vo, D.V. N. (2016). Influence of lanthanide promoters on Ni/SBA-15 catalysts for syngas production by methane dry reforming. *Procedia Engineering, 148*, 1388–1395.

Pakhare, D. and Spivey, J. (2014). A review of dry (CO_2) reforming of methane over noble metal catalysts. *Chemical Society Reviews, 43*, 7813–7837.

Pechimuthu, N. A., Pant, K. K. and Dhingra, S. C. (2007). Deactivation studies over Ni-K/CeO_2-Al_2O_3 catalyst for dry reforming of methane. *Industrial and Engineering Chemistry Research, 46(6)*, pp. 1731–1736.

Rahemi, N., Haghighi, M., Babaluo, A. A., Allahyari, S. and Jafari, M. F. (2014). Syngas production from reforming of greenhouse gases CH_4/CO_2 over Ni–Cu/Al_2O_3 nanocatalyst: Impregnated vs. plasma-treated catalyst. *Energy Conversion and Management, 84*, 50–59.

Rostrup-Nielsen, J. R. (1997). Industrial relevance of coking. *Catalysis Today, 37(3)*, pp. 225–232.

Saraswat, S. K. and Pant, K. K. (2013). Synthesis of carbon nanotubes by thermo catalytic decomposition of methane over Cu and Zn promoted Ni/MCM-22 catalyst. *Journal of Environmental Chemical Engineering, 1(4)*, pp. 746–754.

Selvarajah, K., Phuc, N. H., Abdullah, B., Alenazey, F. and Vo, D.-V. N. (2016). Syngas production from methane dry reforming over Ni/Al_2O_3 catalyst. *Research on Chemical Intermediates, 42(1)*, pp. 269–288.

Serrano-Lotina, A. and Daza, L. (2014). Influence of the operating parameters over dry reforming of methane. *International Journal of Hydrogen Energy, 39*, 4089–4094.

Therdthianwong, S., Siangchin, C. and Therdthianwong, A. (2008). Improvement of coke resistance of Ni/Al_2O_3 catalyst in CH_4/CO_2 reforming by ZrO_2 addition. *Fuel Processing Technology, 89(2)*, pp. 160–168.

Usman, M., Wan Daud, W. M. A. and Abbas, H. F. (2015). Dry reforming of methane: Influence of process parameters—A review. *Renewable and Sustainable Energy Reviews, 45*, 710–744.

Wolfbeisser, A., Sophiphun, O., Bernardi, J., Wittayakun, J., Föttinger, K., & Rupprechter, G. (2016). Methane dry reforming over ceria-zirconia supported Ni catalysts. *Catalysis Today, 277*, 234–245.

Wu, H., Pantaleo, G., La Parola, V., Venezia, A. M., Collard, X., Aprile, C. and Liotta, L. F. (2014). Bi- and trimetallic Ni catalysts over Al_2O_3 and Al_2O_3-MO_x (M=Ce or Mg) oxides for methane dry reforming: Au and Pt additive effects. *Applied Catalysis B: Environmental, 156–157*, 350–361.

Xu, J., Zhou, W., Wang, J., Li, Z. and Ma, J. (2009). Characterization and analysis of carbon deposited during the dry reforming of methane over Ni/La_2O_3/Al_2O_3 catalysts. *Chinese Journal of Catalysis, 30(11)*, pp. 1076–1084.

Zhang, J., Wang, H. and Dalai, A. K. (2008). Effects of metal content on activity and stability of Ni-Co bimetallic catalysts for CO_2 reforming of CH_4. *Applied Catalysis A: General, 339(2)*, pp. 121–129.